E11-2024-56

A. M. Chervyakov *

FEM-BASED APPROACHES TO MODELING THE RESOURCE-DEMANDING MAGNETOSTATIC PROBLEMS WITH MAGNETIC SCALAR POTENTIAL

Submitted to “Electromagnetic Science”

* E-mail: acher@jinr.ru

Червяков А. М. E11-2024-56

О конечно-элементном моделировании ресурсно-затратных задач магнитостатики с помощью скалярного потенциала

Целью работы является повышение эффективности конечно-элементного моделирования магнитных полей в ресурсно-затратных задачах магнитостатики с постоянными токами и нелинейными магнитными материалами. Предложены новые подходы, в которых для численного анализа уравнений Максвелла в методе конечных элементов используется полный скалярный потенциал, а индукционный эффект проводников с током моделируется с помощью как скачков потенциала на разрезах, так и намагниченностей линейных и нелинейных постоянных магнитов. Для проверки предложенных методов проводится конечно-элементное моделирование магнитных полей для дипольного магнита с токопроводящей катушкой. Сравнение с референсным моделированием на основе магнитного векторного потенциала демонстрирует значительное сокращение как объема оперативной памяти, так и времени вычислений при аналогичной точности результатов.

Работа выполнена в Лаборатории информационных технологий им. М. Г. Мещерякова ОИЯИ.

Препринт Объединенного института ядерных исследований. Дубна, 2024

Chervyakov A. M. E11-2024-56

FEM-Based Approaches to Modeling the Resource-Demanding Magnetostatic Problems with Magnetic Scalar Potential

The paper aims to improve the computational efficiency of 3D finite-element method for modeling the resource-demanding magnetization problems in the presence of steady currents and nonlinear magnetic materials. For this purpose, new approaches based on the use of magnetic scalar potential for numerical analysis of Maxwell's equations and modeling the inductive effect of conductors using both the scalar potential discontinuities of thin cuts and the magnetizations of linear and nonlinear permanent magnets are proposed and validated. Compared to the computationally expensive standard approach for modeling magnetic fields in dipole magnet with magnetic vector potential and the current-carrying coil, the novel approaches allow us to obtain the expected results with similar accuracy at much lower computational cost.

The investigation has been performed at the Meshcheryakov Laboratory of Information Technologies, JINR.

Preprint of the Joint Institute for Nuclear Research. Dubna, 2024

INTRODUCTION

Despite the excellent quality of numerical calculations, 3D finite-element analysis of magnetic fields with magnetic vector potential as a primary unknown becomes computationally demanding for magnetostatic problems involving complicated model geometries, large nonconducting regions and nonlinear materials. Obtaining accurate results for these problems is therefore either limited or elongated by the available hardware resources, thus hindering the efficiency of the solution.

While the use of the magnetic vector potential as a fundamental unknown for computation of magnetic fields caused by steady currents is commonly adopted in numerical magnetostatics [1–3], its extension to the whole problem domain, including large nonconducting regions, unnecessarily increases the total number of the model degrees of freedom, thus leading to either higher memory consumption or longer processing times. In fact, the current-free regions can be modeled much more economically by using the total scalar potential instead of the vector potential while leaving the current-carrying regions for the use of the magnetic vector potential and coupling both potentials together on their common interfacing boundaries [4–10]. For consistency of combined formulation with Ampere's law, the nonconducting regions must be made however simply connected. This can be ensured via constructing thin cuts to prevent all paths from linking the currents and imposing across each cut surface a scalar potential discontinuity equal to the fraction of the enclosed current. In this way, the computational efficiency of the finite-element method for solving the resource-demanding magnetostatic problems in the presence of steady currents and nonlinear magnetic materials can be considerably improved [11, 12]. Moreover, such problems can be solved by using the magnetic scalar potential alone when it is only necessary to compute the field distributions in the current-free regions of the problem domain and not inside the conductors. To this end, the inductive effect of conductors to produce the magnetic fields can be modeled by using either the scalar potential discontinuities as in the vector-scalar formulation [13–15] or the magnetization of linear and nonlinear permanent magnets similarly to the development of mechanical antenna propagation [16]. Both can represent equally well the magneto-motive forces of conductors, thereby allowing either thin cuts or permanent magnets to substitute the impact of conductors on the nonconducting regions.

The benchmarking of these approaches based entirely on the magnetic scalar potential against the standard approach using the magnetic vector potential is the purpose of this paper. The computation of the field distributions is illustrated by using the model of dipole magnet [17] as an example. To properly deflect, focusing, or correcting the beam of particles in the particle accelerators, the magnet design and optimization are usually dominated by the requirements of the extremely uniform fields of the order of 10^{-4} of the field amplitude [17, 18]. The precise position of the coil, the wires inside the coil and the pole profiles are therefore the important geometrical aspects influencing the field calculations. The magnetostatic field equations are solved for the magnetic scalar potential in nonconducting regions, where the inductive effect of conductors is modeled either with the help of the scalar potential jumps across thin cuts or by using the magnetization of linear and nonlinear permanent magnets. The analysis of numerical efficiency of novel approaches is carried out via comparison with the standard approach for the same modeling example of dipole magnet [11, 12]. Due to substantial reduction in computational effort, these methods are well-suited for the finite-element modeling of magnetic systems, where many simulations with significant variation in geometric shapes are required during the development of the optimal system design.

1. MODELING FRAMEWORK FOR USE OF SCALAR POTENTIAL

In general, static magnetic fields are caused by either steady currents or permanent magnets. The paper focuses on solving the magnetostatic problems with source currents, while using permanent magnets complementary to substitute the currents impact and simplify the solution. For these problems, the magnetic field strength $\mathbf{H}$ and the magnetic flux density $\mathbf{B}$ are described by the following set of Maxwell's equations [19]:

$$\nabla \times \mathbf{H} = \mathbf{J} \quad \text{and} \quad \nabla \cdot \mathbf{B} = 0 \text{ in } \Omega, \tag{1}$$

where $\mathbf{H}$ and $\mathbf{B}$ are three-component vector functions to be defined in a three-dimensional domain Ω. The current density $\mathbf{J}$ is solenoidal ($\nabla \cdot \boldsymbol{j} = 0$) in the case of applied currents and is zero ($\mathbf{J} = \mathbf{0}$) for permanent magnets. The magnetic properties of materials involved in the problem domain Ω are accounted for via the appropriate constitutive relations between the flux density $\mathbf{B}$ and the field strength $\mathbf{H}$ describing either linear or nonlinear behavior of the magnetization curves. Assuming all materials to be isotropic, these relations are expressed respectively as

$$\mathbf{B} = \mu_0 \mu_r \mathbf{H} \quad \text{and} \quad \mathbf{B} = f(H)\, \mathbf{H}/H, \tag{2}$$

where μ_0 is the permeability of a free space, whereas μ_r and $f(H)$ are the relative permeability and the nonlinear magnetization curve specified for each

material. In turn, the following constitutive relations describe respectively the magnetic properties of linear and nonlinear permanent magnets:

$$\mathbf{B} = \mu_0 \mu_{\mathrm{rec}} \mathbf{H} + \mathbf{B}_r \quad \text{and} \quad \mathbf{B} = f(H_s)\, \mathbf{H}_s / H_s, \tag{3}$$

where μ_{rec} is the recoil permeability, $\mathbf{B}_r = \mu_0 \mu_{\mathrm{rec}} \mathbf{H}_c$ the remanent flux density, $\mathbf{H}_s = \mathbf{H} + \mathbf{H}_c$ the shifted magnetic field, and $\mathbf{H}_c$ the coercivity which is the intensity of the reversely applied magnetic field capable of fully demagnetizing the magnet.

A typical geometry of the computational domain Ω consists of the current-carrying region Ω_c, where the current density $\mathbf{J}$ is accommodated, and the current-free region Ω_n, where the current density $\mathbf{J}$ is zero and where the magnetic field is usually computed (see Fig. 1).

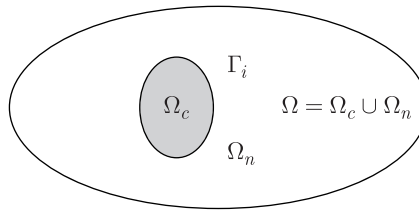

Fig. 1. Typical computational domain of a magnetostatic problem

Following the standard approach [1–3], the set of equations (1) can be solved in the entire problem domain Ω for magnetic vector potential $\mathbf{A}$ via the substitution $\mathbf{B} = \boldsymbol{\nabla} \times \mathbf{A}$. However, the first equation of the system (1) in the current-free region Ω_n is simplified to the form

$$\boldsymbol{\nabla} \times \mathbf{H} = \mathbf{0} \quad \text{in} \quad \Omega_n \tag{4}$$

and, therefore, can be solved instead by introducing the magnetic scalar potential V_m as

$$\mathbf{H} = -\boldsymbol{\nabla} \cdot V_m \quad \text{in } \Omega_n. \tag{5}$$

The potential V_m is defined by a second-order differential equation of Laplace's type obtained from the second equation of the system (1) after successive substitutions of the constitutive relations (2) or (3) and equation (5). Combining these relations together for brevity as $\mathbf{B} = \mathbf{B}[\mathbf{H}]$ yields the governing equation in terms of the scalar potential,

$$\boldsymbol{\nabla} \cdot \mathbf{B}\,[-\boldsymbol{\nabla} V_m] = 0 \quad \text{in} \quad \Omega_n. \tag{6}$$

The boundary conditions imposed on the potential V_m ensure continuity of the normal component of the vector $\mathbf{B}$ and the tangential component of the vector $\mathbf{H}$ across the boundary $\partial\Omega_n$ as follows:

$$\mathbf{n} \cdot \mathbf{B}[-\boldsymbol{\nabla} V_m] = 0 \quad \text{on} \quad \Gamma_b, \tag{7}$$

$$V_m = 0 \quad \text{on } \Gamma_h, \tag{8}$$

where Γ_b and Γ_h are the two parts of the entire boundary $\partial\Omega_n = \Gamma_b \bigcup \Gamma_h$ and $\mathbf{n}$ is the outward normal to $\partial\Omega_n$. Conditions (7) and (8) preserve also symmetry, or anti-symmetry of the model by enforcing the flux density $\mathbf{B}$ to be tangential to Γ_b, or the magnetic field $\mathbf{H}$ normal to Γ_h.

To reduce the total number of the model degrees of freedom, it is therefore preferable to solve the set of three-dimensional equations (1) for magnetic scalar potential V_m in the region Ω_n, while leaving the magnetic vector potential $\mathbf{A}$ for the use in the region Ω_c and coupling both potentials together on their common interfacing boundary. However, the potential V_m becomes discontinuous for applications where the region Ω_c with a hole representing, for example, a circular current-carrying coil is surrounded by the region Ω_n. For such a geometry of the model, the region Ω_n becomes multiply connected where the potential V_m is globally multivalued due to Ampere's law (see Fig. 2).

The ambiguity with scalar potential can be resolved as shown in Fig. 2 via constructing thin cut to prevent any loop from linking the current and thereby make a nonsimply connected region Ω_n simply connected. Simultaneously, a scalar potential discontinuity ΔV_m equal to the value of the enclosed current I is imposed over two different sides of the cut surface in the agreement with Ampere's law,

$$\Delta V_m = V_m^+ - V_m^- = I \quad \text{on} \quad \Gamma_{\text{cut}}. \tag{9}$$

With Eq. (9), the combined formulation can be solved consistently by the finite-element method, provided that both potentials are properly coupled together on their common interfacing boundary [11, 12]. For resource-demanding magnetization problems with large nonconducting regions, the use of combined potentials can substantially reduce computational effort as compared to the approach based entirely on the magnetic vector potential (see paper [12] for comparison).

An important conclusion behind the cut construction stems from the fact that the magnetic fields involved in the current-free region Ω_n are generated

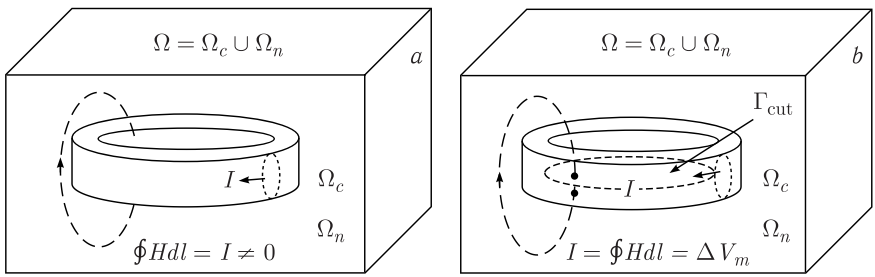

Fig. 2. A circular coil carrying the current I with and without thin cut Γ_{cut}. *a*) The scalar potential V_m defined by Eq. (5) is multivalued in Ω_n due to Ampere's law with no cut. *b*) Imposing thin cut Γ_{cut} with a discontinuity I in V_m from one side of the cut surface to the other makes the scalar potential V_m single-valued on the cut complement

by the prescribed discontinuity in the magnetic scalar potential replicating the coil current according to Eq. (9). In fact, there exists a surface current density $\mathbf{J} = \delta(n) \cdot \mathbf{K}$ which enforces the tangential discontinuity in $\mathbf{H}$-field on the cut surface due to Ampere's law,

$$-\mathbf{n} \times \mathbf{H} = \mathbf{n} \times \boldsymbol{\nabla} \cdot V_m = \mathbf{K} \quad \text{on} \quad \Gamma_{\text{cut}}, \tag{10}$$

where $\mathbf{n}$ is the outward normal to the surface of discontinuity. Integrating (10) over the contours on this surface recovers Eq. (9). It becomes therefore possible to extend the use of the magnetic scalar potential V_m to the whole problem domain Ω by replacing the inductive effect of the coil current with the potential jump of thin cut equivalent to magneto-motive force (MMF) of conductor.

The two approaches are proposed to compute the magnetostatic fields solely in terms of scalar potential in this paper. In the first, the coil current is substituted with the potential jump of thin cut, while in the second, with the magnetization of permanent magnet. Although the coil is no longer included in the computation, its model is accounted for via constructing thin cut and permanent magnet to reproduce the impact of the coil current correctly. In the agreement with previous formulations, the model of circular coil represented as a homogenized current-carrying body with the geometry of the hollow cylinder is used for construction of thin cut and permanent magnet (see Fig. 3, *a*).

According to this coil model, a single cut plane forming a circle with the diameter equal to the averaged coil diameter is constructed and placed at the middle of the coil length to substitute the coil impact in the first approach (see Fig. 3, *b*). In the second, the geometry of permanent magnet forming a circular cylinder with averaged coil diameter is constructed and placed at the center of the coil over its full length to reproduce the same coil impact (see Fig. 3, *c*).

By construction, the cut surface and permanent magnet are passing through various material regions of the model domain specified by either the relative permeabilities or the nonlinear magnetization curves (see Eq. (2)). The corresponding parts of the cut surface are then assigned with material

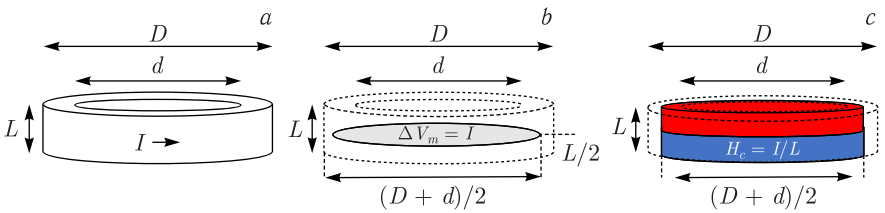

Fig. 3. Substituting coil current with thin cut and permanent magnet: *a*) model of a circular coil represented as a homogenized current-carrying body; *b*) equivalent model of thin cut with the potential jump $\Delta V_m = I$ determined by the coil current; *c*) equivalent model of permanent magnet with coercivity $H_c = I/L$ determined by MMF of the coil

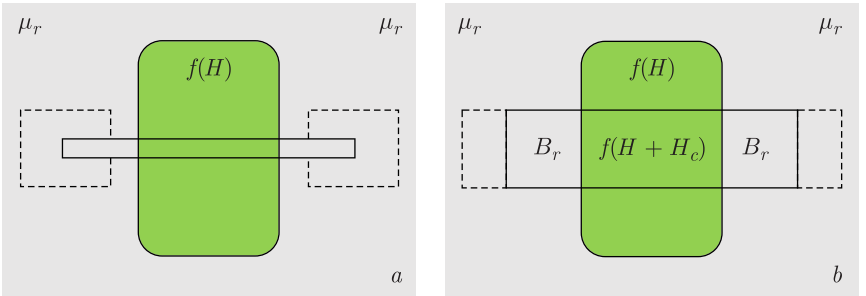

Fig. 4. Different magnetization models for *a*) cut surface and *b*) permanent magnet associated with different material properties of the crossed regions

properties of the crossed regions (see Fig. 4, *a*). In turn, the parts of permanent magnet passing through material regions specified by the constant relative permeabilities are associated with the linear permanent magnets (see Eq. (3)) and specified by the remanent flux densities $B_r = \mu_0 \mu_r H_c$ with the coercivity H_c determined from MMF of the coil (see Fig. 4, *b*). The other parts passing through regions of ferromagnetic materials specified by nonlinear BH-curves $f(H)$ are associated with the nonlinear permanent magnets (see Eq. (3)) and assigned with the demagnetization curves obtained via shifting the BH-curves of the crossed regions by the value of coercivity H_c to the left. The remanent flux densities $B_r = f(H_c)$ for nonlinear permanent magnets are defined as the values of the demagnetization curves at $H = 0$ (see Fig. 4, *b*).

Although constructing thin cut and permanent magnets adds modeling complexity to the problem, it is far overweighed by computational benefits of using the magnetic scalar potential for its solution.

2. BENCHMARKING SCALAR POTENTIAL FOR FIELD COMPUTATION

To benchmark the numerical potential of the novel approaches in terms of magnetic scalar potential (MSP) against the standard formulation with magnetic vector potential (MVP), we use the model of dipole magnet [17]. The model consists of two poles arranged in parallel at equal distances above and below the median plane of large spherical air domain used for magnetic insulation. Either pole of the magnet includes the circular coil driven by the DC current, as well as the yoke, four spiral sectors and other constituents made of nonlinear ferromagnetic materials (see Fig. 5).

The model possesses three planes of symmetry allowing us to truncate its geometry and reduce the computational cost. We explore only the 1/8th part of the model geometry to obtain the results for the entire model. The mirror symmetry is used to cut the geometry along the median plane and impose boundary conditions ensuring the tangential continuity of the **B**-field (see Eq. (8)), whereas the fourfold axial symmetry allows us to cut the remaining parts of the geometry along the (zx) and (zy) planes and impose boundary

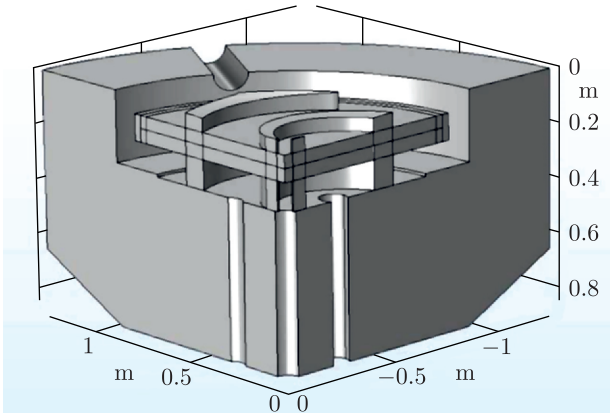

Fig. 5. The 1/8th part of unified geometry of dipole magnet used in FEM simulation of magnetic fields generated by three equivalent sources shown in the picture: coil, thin cut, and permanent magnet

conditions ensuring the normal continuity of the **B**-field (see Eq. (7)) on the potentials in both formulations. The role of these boundary conditions is to mimic the entire geometry while exploiting its 1/8th part.

The geometry of the circular coil represents an axisymmetric hollow cylinder formed by rotation around the z axis of a rectangle lying in the (zx) plane. The coil is assumed to be of the multiturn type and therefore modeled as a homogenized current-carrying body with multiple wires arranged and placed in a potting material (see Fig. 6). The excitation DC current is applied to the coil cross-section boundary. A coil numeric analysis is made prior to the field calculation to compute the magnitude and direction of the current flow inside conductor.

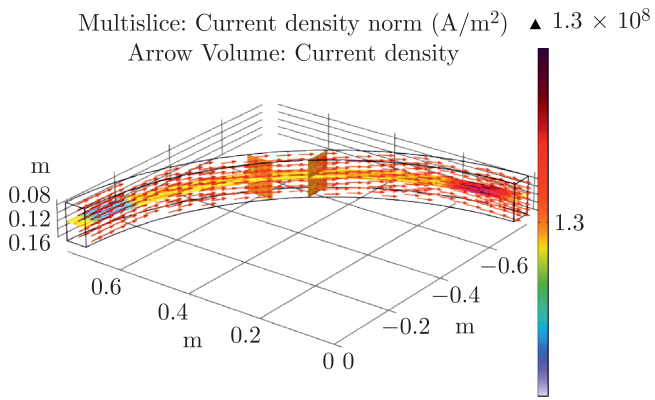

Fig. 6. Distribution of the current density inside the homogenized multiturn coil

The geometry of insulating air domain represents a large sphere surrounded by the boundary layer, whose thickness is scaled towards infinity to mimic virtually the infinite element domain. Additionally, the geometries of the cut surface and permanent magnet are constructed and added to the air domain when the magnetic scalar potential is used. In the MVP formulation, the magnetic vector potential is applied to the whole computational domain of the model. However, in the MSP formulations with the cut surface and permanent magnet, the magnetic scalar potential is instead applied while a circular coil is not modelled.

Three studies based on the same model geometry (see Fig. 5) are performed and compared with COMSOL Multiphysics software [20]. The first uses the MVP formulation to obtain the reference results with excellent accuracy. The second and third repeat similar computations by using the two MSP formulations with cut surface and permanent magnet for validation. The main

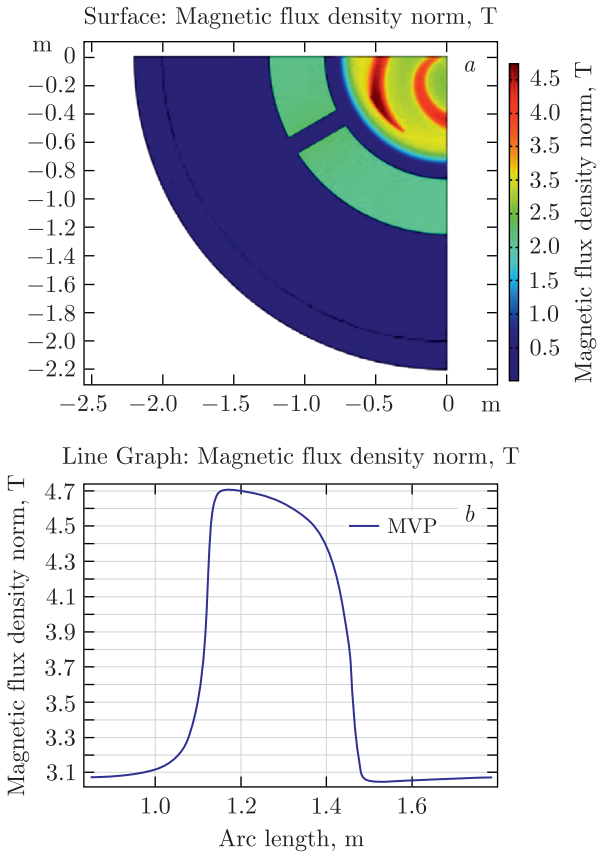

Fig. 7. Reference magnetic field distributions *a*) over the median plane and *b*) along the azimuthal direction

quantities of interest are the field distributions over the median plane, as well as along the azimuthal direction of the aperture area. For FEM analysis of each study, the conforming mesh is generated with almost the same number of finite elements, despite the fact that the additional constructions of thin cut and permanent magnet are added to the geometry of the model. The minimal mesh quality is optimized to ensure the convergence and stability of solutions. The edge and Lagrange shape functions up to third order are used for approximation of magnetic vector and scalar potentials, respectively [21–23]. The direct PARDISO solver based on multifrontal factorization of the stiffness matrix [24] is used for all studies to find numerical solutions for the potentials. In the MVP formulation, the gauge fixing for **A**-field is used together with the direct solver as the necessary condition to ensure the convergence of solution [25]. In the MSP formulation with thin cut, the magnetic field outside

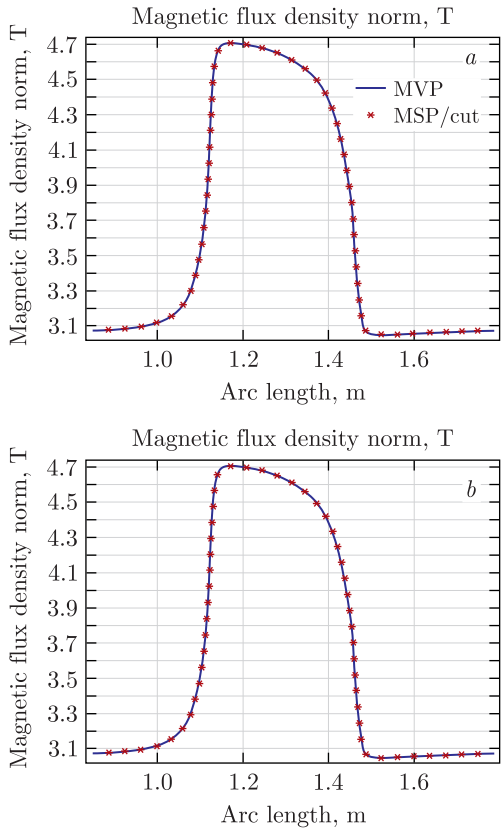

Fig. 8. Field distributions along the azimuthal direction. The solid curve refers to the reference field and the points refer to fields calculated using the MSP formulation with *a*) the permanent magnet and *b*) the cut surface

the coil region is obtained by solving first for magnetic scalar potential and then taking the negative gradient from the solution result. For this reason, the scalar potential discontinuity across the cut surface does not violate the continuity of the magnetic field. The simulation results are shown in Figs. 7 and 8 and summarized in the table.

Summary of formulations used for modeling of dipole magnet

Formulation	Element order	Number of FEs	Number of DOFs	Memory (Gb) Phys/Virtual	Time of computation	Number of iterations
MSP/PM	3	473 087	2 244 400	25.34/43.15	5 m 19 s	8
MSP/cut	3	438 289	2 095 098	22.97/40.47	6 m 12 s	11
MVP	3	414 840	9 958 301	367.35/414.06	4 h 19 m 8 s	8

Both MSP formulations with thin cut and permanent magnet demonstrate a satisfactory qualitative and quantitative agreement with the standard MVP formulation. The relative errors amount to the maximum of only 7 and 5 G, respectively, as compared to the reference results. On the other hand, these formulations require much less computational resources for finite-element modeling of dipole magnet. The reduction of the total number of DOFs amounts to a factor of 4.5, the random-access memory to a factor of 15, and the computation time to a factor of 40.

CONCLUSIONS

In this paper, we proposed the novel approaches for finite-element analysis of magnetostatic fields in terms of magnetic scalar potential where the inductive effect of conductors is modeled by using either scalar potential discontinuities of thin cuts or the magnetization of permanent magnets. The numerical performance of the proposed methods is assessed against the standard approach based on magnetic vector potential, whose capability of providing the excellent quality results is well-known. For modeling of dipole magnet, the comparison demonstrates a substantial reduction in the computational cost at almost similar accuracy of computations. For this reason, the novel approaches can be especially well-suited for finite-element modeling of those magnetic systems where many simulations with significant variation in geometric shapes are required to develop the optimal system design.

Acknowledgements. The computational support from HybriLIT Heterogeneous Computing Platform (MLIT, JINR) is acknowledged.

REFERENCES

1. *Bedrosian G.* High-Performance Computing for Finite Element Methods in Low-Frequency Electromagnetics // Prog. Electromagn. Res. 1993. V. 7. P. 57–110.
2. *Monk P.* Finite Element Method for Maxwell's Equations. Oxford: Clarendon Press, 2003.

3. *Volakis, J. L., Chatterjee A., Kempel L.C.* Finite Element Method for Electromagnetics. New York: Wiley-IEEE, 1998.
4. *Guerin C., Tanneau G., Meunier G., Brunotte X., Albertini J. B.* Three Dimensional Magnetostatic Finite Elements for Gaps and Iron Shells Using Magnetic Scalar Potentials // IEEE Trans. Magn. 1994. V. 30. P. 2885–2888.
5. *Gross P. W., Kotiuga P. R.* Electromagnetic Theory and Computation: A Topological Approach. Cambridge: Cambridge Univ. Press, 2004.
6. *Leonard P. J., Rodger D.* A New Method for Cutting the Magnetic Scalar Potential in Multiply Connected Eddy Current Problems // IEEE Trans. Magn. 1989. V. 25. P. 4132.
7. *Rodger D., Eastham J.* Multiply Connected Regions in the $A - \psi$ Three-Dimensional Eddy-Current Formulation // IEE Proc. A, Phys. Sci. Meas. Instrum. Manage. Educ. Rev. 1987. V. 134. P. 58.
8. *Biro O., Preis K.* On the Use of the Magnetic Vector Potential in the Finite Element Analysis of Three-Dimensional Eddy Currents // IEEE Trans. Magn. 1989. V. 25. P. 3145–3159.
9. *Biro O., Preis K., Richter K. R.* On the Use of the Magnetic Vector Potential in the Nodal and Edge Finite Element Analysis of 3D Magnetostatic Problems // IEEE Trans. Magn. 1996. V. 32. P. 651–654.
10. *Stockrahm A., Lahtinen V., Kangas J. J. J., Kotiuga P. R.* Cuts for 3D Magnetic Scalar Potentials: Visualizing Unintuitive Surfaces Arising from Trivial Knots. physics.comp-ph/arXiv:1902.01124v2. 2019.
11. *Chervyakov A.* On the Use of Mixed Potential Formulation for Finite-Element Analysis of Large-Scale Magnetization Problems with Large Memory Demand. arXiv:2307.12308v1[physics. comp-ph]. 2023.
12. *Chervyakov A. M.* On Finite-Element Modeling of Large-Scale Magnetization Problems with Combined Magnetic Vector and Scalar Potentials // Phys. Part. Nucl. Lett. 2024. V. 21. P. 1074–1083.
13. *Crawford C. B.* The Physical Meaning of the Magnetic Scalar Potential and Its Use in the Design of Hermetic Electromagnetic Coil // Rev. Sci. Instrum. 2021. V. 92. P. 1–8.
14. *Chervyakov A.* Comparison of Magnetic Vector and Total Scalar Potential Formulations for Finite-Element Modeling of Dipole Magnet with COMSOL Multiphysics. arXiv:2107.01957[physics.comp-ph]. 2021.
15. *Chervyakov A.* Finite-Element Modelling of Magnetic Fields for Superconducting Magnets with Magnetic Vector and Total Scalar Potentials Using COMSOL Multiphysics® // Int. J. Eng. Syst. Model. Simul. 2022. V. 13. P. 117–133.
16. *Wang X., Zhang W., Zhou X., Cao Z., Quan X.* Research on Permanent Magnet-Type Super-Low-Frequency Mechanical Antenna Communication // Int. J. Antenn. Propag. 2021. V. 55244732. P. 1–16.
17. *Karamysheva G. et al.* Compact Superconducting Cyclotron SC200 for Proton Therapy // Proc. of 23rd Int. Conf. on Cyclotrons and Their Applications. Zurich, 2016. P. 371–373.
18. *Kleeven W., Zarembo S.* Cyclotrons: Magnetic Design and Beam Dynamics. physics.med-ph/arXiv:1804.08961. 2018.
19. *Jackson J. D.* Classical Electrodynamics. 3rd ed. New York: John Wiley & Sons, 1998.
20. *COMSOL Multiphysics*®. COMSOL AB. Stockholm, 2018.

21. *Mur G.* Edge Elements, Their Advantages, and Their Disadvantages // IEEE Trans. Magn. 1994. V. 30. P. 3552–3557.
22. *Boffi D., Gastaldi L.* Edge Finite Elements for the Approximation of Maxwell Resolvent Operator // Math. Model. Numer. Anal. 2002. V. 36. P. 293–305.
23. *Kamireddy D., Nandy A.* A Novel Conversion Technique from Nodal to Edge Finite Element Data Structure for Electromagnetic Analysis. math.NA/arXiv:2103. 15379v1. 2021.
24. *Schenk O., Gartner K., Fichtner W., Stricker A.* PARDISO: A High-Performance Serial and Parallel Sparse Linear Solver in Semiconductor Device Simulation // Future Gener. Comput. Syst. 2001. V. 18. P. 69–78.
25. *Creuse E., Dular P., Nicaise S.* About Gauge Conditions Arising in Finite Element Magnetostatic Problems // Comput. Math. Appl. Elsevier, 2019. V. 77. P. 1563–1582.

Received on November 20, 2024.

Редактор *Е. И. Кравченко*

Подписано в печать 11.12.2024.
Формат 60 × 90/16. Бумага офсетная. Печать цифровая.
Усл. печ. л. 0,75. Уч.-изд. л. 0,48. Тираж 100 экз. Заказ № 60999.

Издательский отдел Объединенного института ядерных исследований
141980, г. Дубна, Московская обл., ул. Жолио-Кюри, 6.
E-mail: publish@jinr.ru
www.jinr.ru/publish/